

Low-Temperature Soft-Cover-Assisted Hydrolysis Deposition of Large-Scale TiO₂ Layer for Efficient Perovskite Solar Modules

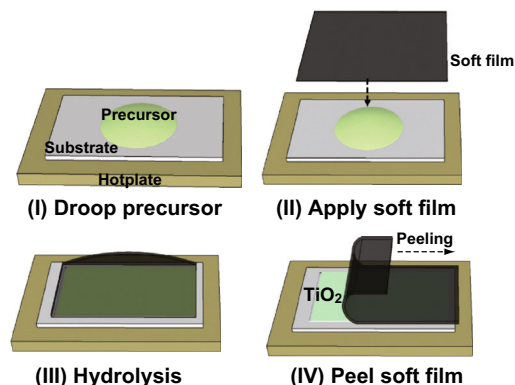
Jinjin He¹ · Enbing Bi¹ · Wentao Tang¹ · Yanbo Wang¹ · Xudong Yang^{1,2} · Han Chen^{1,2} · Liyuan Han¹

Received: 1 March 2018 / Accepted: 4 April 2018 / Published online: 30 April 2018
© The Author(s) 2018

Highlights

- A simple soft-cover-assisted hydrolysis method to prepare TiO₂ films at a low temperature is proposed.
- Compact homogeneous large-area TiO₂ films with a needle-like morphology were obtained.
- A solar module fabricated with as-prepared TiO₂ films as electron transfer layers exhibited a power conversion efficiency of 14.01%.

Abstract Perovskite solar cells with TiO₂ electron transport layers exhibit power conversion efficiency (PCE) as high as 22.7% in single cells. However, the preparation process of the TiO₂ layer is adopted by an unscalable method or requires high-temperature sintering, which precludes its potential use for mass production of flexible devices. In this study, a scalable low-temperature soft-cover-assisted hydrolysis (SAH) method is presented, where the precursor solution is sandwiched between a soft cover and preheated substrate to form a closed hydrolysis environment. Compact homogeneous TiO₂ films with a needle-like structure were obtained after the hydrolysis of a



Electronic supplementary material The online version of this article (<https://doi.org/10.1007/s40820-018-0203-7>) contains supplementary material, which is available to authorized users.

✉ Han Chen
chen.han@sjtu.edu.cn

✉ Liyuan Han
han.liyuan@sjtu.edu.cn

¹ State Key Laboratory of Metal Matrix Composites, School of Material Science and Engineering, Shanghai Jiao Tong University, 800 Dong Chuan Road, Shanghai 200240, People's Republic of China

² Materials Genome Initiative Center, Shanghai Jiao Tong University, 800 Dong Chuan Road, Shanghai 200240, People's Republic of China

TiCl₄ aqueous solution. Moreover, by careful optimization of the TiO₂ fabrication conditions, a high PCE of 14.01% could be achieved for a solar module (4 × 4 cm²) prepared using the SAH method. This method provides a novel approach for the efficient scale-up of the low-temperature TiO₂ film growth for industrial applications.

Keywords Low-temperature · TiO₂ · Large-scale · Soft-cover-assisted hydrolysis deposition · Perovskite solar cell

1 Introduction

Perovskite solar cells (PSCs) have been demonstrated to be next-generation photovoltaic devices that meet future energy-generation demands owing to their high power conversion efficiency (PCE), low cost, simple solution-based preparation, lightweight, and flexibility [1–6]. Conventional PSCs using TiO_2 as the electron transport material have exhibited high PCEs [7–10]. However, the high-temperature processing of the TiO_2 layer makes their manufacture more complex and hampers the development of lightweight and flexible substrates. To overcome this limitation, several deposition techniques to fabricate TiO_2 films at low temperatures have been successfully implemented, such as spin coating (SC) [11–13], atomic layer deposition (ALD) [14, 15], sputtering [16–18], chemical bath deposition [19, 20], and electron-beam evaporation [21].

Among these techniques, SC is the principal method for low-temperature TiO_2 film preparation. A PSC based on a TiO_2 layer prepared by SC chlorine-capped TiO_2 colloidal nanocrystal solutions has achieved a PCE of 19.5%, with an active area of 1.1 cm^2 , which is the highest PCE reported for PSCs prepared at low temperatures [22]. Non-SC methods, including ALD, sputtering, chemical bath deposition, and electron-beam evaporation, are also applicable for controllable TiO_2 film deposition and have achieved PCEs up to 19% for active areas smaller than 1 cm^2 [7]. However, it is obvious that neither SC nor above non-SC methods are suitable for a large-scale PSC manufacture owing to their inherent limitations [23, 24]. Therefore, the investigation of simple TiO_2 -layer preparation methods involving a large area and low temperatures is necessary for industrial applications.

In this study, we report a simple low-temperature soft-cover-assisted hydrolysis (SAH) method, where a soft polyimide (PI) film is used to cover a TiCl_4 aqueous solution spread on a preheated substrate. Compact and homogeneous large-area TiO_2 films with a needle-like morphology (SAH- TiO_2) were obtained after the hydrolysis. Moreover, a solar module ($4 \times 4 \text{ cm}^2$) with an SAH- TiO_2 layer as an electron transport layer using the SAH method exhibited a PCE of 14.01% in a conventional device configuration at low temperatures. Therefore, the proposed SAH technology provides a novel non-SC route to the deposition of large-area TiO_2 films for industrial applications.

2 Experimental Methods

2.1 Materials and Reagents

All chemicals were used as received. PbI_2 (99%), *N,N*-dimethylformamide (anhydrous), dimethyl sulfoxide, and chlorobenzene were purchased from Sigma Aldrich. Methylammonium iodide (98%) was obtained from Tokyo Chemical Industry Co. Ltd. Titanium tetrachloride (TiCl_4) was purchased from Alfa Aesar. A low-temperature TiO_x SC solution was purchased from Shanghai MaterWin New Materials Co., Ltd.

2.2 Preparation of an SAH- TiO_2 Layer

The substrates were cleaned by a detergent followed by sequential ultrasonic washing in deionized water, ethanol, and acetone (for 30 min in each of them); they were then dried under nitrogen gas. After 15 min of oxygen plasma treatment, the substrates were preheated at $75 \text{ }^\circ\text{C}$ for 10 min on a heating plate. Different concentrations (0.1–0.6 M) of $25 \mu\text{L cm}^{-2}$ TiCl_4 aqueous solution were added at the centers of the substrates, and a piece of a soft film, used as the soft cover, was immediately placed on the precursor. The covered film was peeled off after the hydrolysis for 20 min, followed by washing with deionized water and ethanol; the obtained film was then dried in air.

2.3 Fabrication of PSCs and Modules

A perovskite precursor solution (90 μL) comprising 1.3 M PbI_2 and $\text{CH}_3\text{NH}_3\text{I}$ (1:1/*n*:*n*) in *N,N*-dimethylformamide and dimethyl sulfoxide (4:1/*v*:*v*) was spread on the SAH- TiO_2 film using a consecutive two-step SC process at 1000 and 5000 rpm for 12 and 30 s, respectively. Chlorobenzene (500 μL) was dropped on top of the substrates during the second SC step, 20 s before the end of the procedure, followed by annealing at $100 \text{ }^\circ\text{C}$ for 10 min. A precursor solution of the hole transport layer (HTL) was prepared by dissolving 72.3 mg spiro-OMeTAD, 28.8 μL 4-*tert*-butylpyridine, and 17.5 μL lithium bis(trifluoromethylsulphonyl)imide acetonitrile solution (520 mg mL^{-1}) into 1 mL chlorobenzene. The HTL was then deposited on perovskite by SC at 3000 rpm for 30 s. An 80-nm-thick Au electrode was then thermally evaporated on top of the device to form the back contact. The active area of the device was fixed to 1.02 cm^2 .

For the solar module, the fabricating process was similar to that of small solar cells; the laser scribing patterning process was consistent with that reported previously [25]. In brief, 400 μL TiCl_4 precursor solution was used for a $6 \times 6 \text{ cm}^2$ substrate. For standard control samples, 1.5 mL

TiO_x solution was spin-coated onto a cleaned fluorine-doped tin oxide (FTO) substrate with the same area at 3000 rpm for 30 s. The laser scribing process included scribing on a 4 × 4 cm² FTO/SAH-TiO₂ layer using a 1064-nm laser. A pulse laser with energy of 30 μJ, spot size of 25 μm, pulse frequency of 30 kHz, and low scribing speed of 50 mm s⁻¹ was used to scribe FTO/SAH-TiO₂ substrates with a line width of 100 μm. We then used pulse energy of 10 μJ, spot size of 25 μm, pulse frequency of 20 kHz, and scribing speed of 20 mm s⁻¹ to scribe perovskite/TiO₂ and HTL with a line width of 300 μm. Finally, pulse energy of 10 μJ, spot size of 25 μm, pulse frequency of 35 kHz, and scribing speed of 80 mm s⁻¹ were applied to scribe the Au electrode with a line width of 100 μm.

2.4 Measurement and Characterization

Current–voltage characteristics were measured using a solar simulator (Oriol Class A, 91195A; Newport) and source meter (2400 series; Keithley) at 100 mW cm² and AM 1.5 G illumination. The simulated light intensity was calibrated with a silicon photodiode. The *J*–*V* curves were measured in the reverse (from 1.2 to –0.2 V) or forward (from –0.2 to 1.2 V) scanning modes [26]. The voltage step was fixed at 10 mV, and the delay time (delay at each voltage step before the measurement of the current) was fixed at 50 ms. Monochromatic incident photon-to-current conversion efficiency spectra were measured using a monochromatic incident light (1 × 10¹⁶ photons cm⁻²) in the direct-current mode (CEP-2000BX; Bunko-Keiki). The morphologies and thicknesses of the films were investigated using a field-emission scanning electron microscope (SEM) (JSM-7800F; JEOL). The microstructure of the product was investigated by a field-emission transmission electron microscope (TEM) (JEM-2100F, JEOL). X-ray diffraction (XRD) patterns of the samples were recorded using an X-ray diffractometer (Ultima IV; Rigaku) with Cu K radiation of 1.54 Å and speed of 21° min⁻¹. Ultraviolet–visible (UV–Vis) absorption spectra were recorded using a spectrophotometer (UV-2450; Shimadzu) in a wavelength range of 200–800 nm at room temperature. X-ray spectroscopy measurements were performed using an ESCA-LAB 250Xi spectrometer (Thermo Scientific).

3 Results and Discussion

Schematics of the steps involved in the SAH are shown in Fig. 1. A certain amount of the TiCl₄ precursor solution was dropped onto the preheated substrate at 75 °C (Fig. 1a), and a piece of the soft film was used to cover the liquid precursor (Fig. 1b). The precursor solution spreads

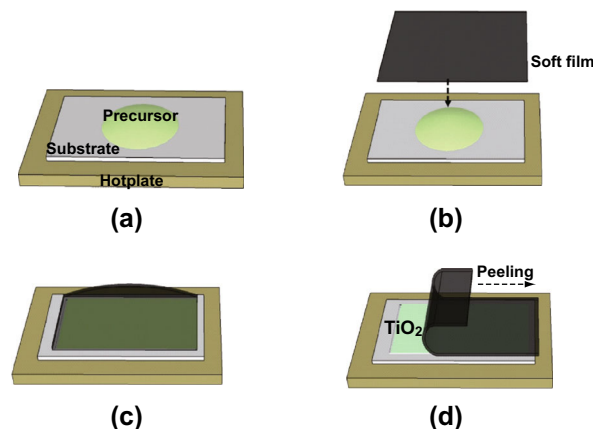


Fig. 1 Schematics of the steps in the SAH

out into a liquid film through the capillary attraction between the precursor solution and soft film (Fig. 1c). A relatively closed environment was formed to prevent rapid evaporation of the solvent into the air. The soft film was then peeled off by a programmed mechanical hand after 20 min of hydrolysis; consequently, a raw TiO₂ film was obtained (Fig. 1d). The deposited substrate was rinsed with water and ethanol successively to remove any loosely bound materials or unreacted precursor solution. According to the features of solution-based underlayer preparation techniques, the flatness of the TiO₂ film in the SAH significantly depended on the uniform liquid film formed during the precursor spreading. This would be related to the wettability of the capped soft film to the precursor solution. A larger wettability implies a larger capillarity between the soft film and solution, which helped form a thin uniform liquid film [27]. The aqueous solution was considered to be the main component used for the hydrolysis; therefore, the candidate soft film should have good wettability with the aqueous solution. Some of the available soft films, such as polyethylene (PE), polyethylene terephthalate (PET), polyvinyl chloride (PVC), and PI films were selected and their contact angles were measured by dropping the aqueous solution onto their surfaces at room temperature in ambient air. As shown in Fig. S1, the average contact angles of the PE, PET, PVC, and PI films were 86°, 81°, 78°, and 52°, respectively. The contact angle of the PI film was significantly smaller than those of the other films; therefore, PI exhibited an excellent wettability with the aqueous solution and was selected as the soft cover for the SAH.

SEM images of the TiO₂ layers on the FTO substrates formed by the SAH using a 0.4-M TiCl₄ aqueous solution are shown in Fig. 2a. The needle-like TiO₂ completely covered the surface of the FTO substrate to form a continuous TiO₂ layer; the resulting SAH-TiO₂ film showed good optical transparency with transmittance larger than

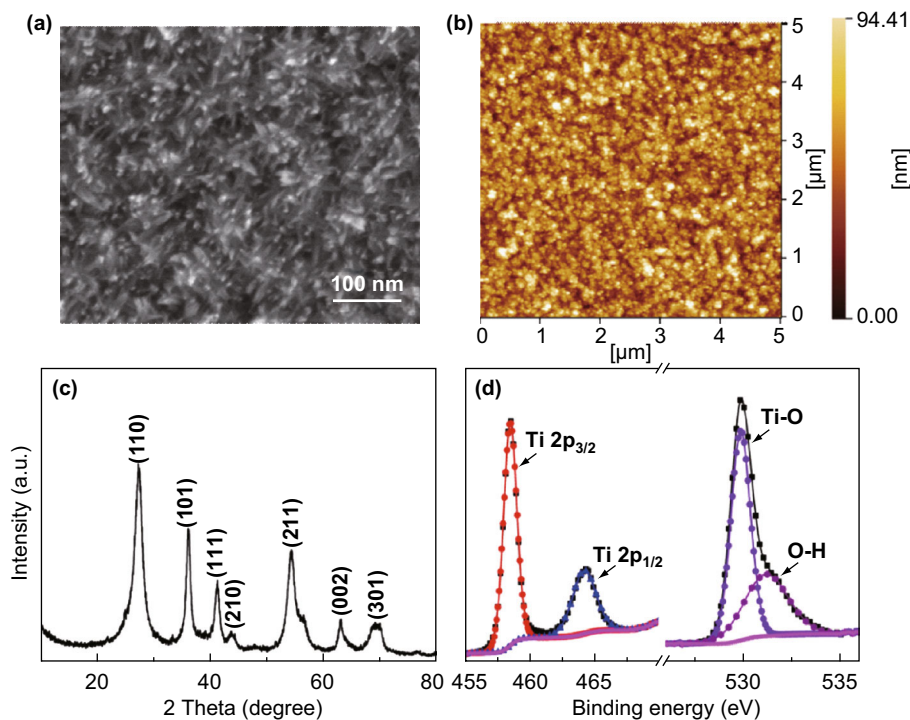


Fig. 2 **a** SEM, **b** AFM images of the TiO_2 films obtained by SAH with a 0.4-M TiCl_4 precursor solution. **c** XRD patterns, **d** XPS results of the TiO_2 material scratched from the TiO_2 film

70% in the visible region (Fig. S2) and uniform current distributions (Fig. S3). Moreover, the size and morphology of the as-prepared TiO_2 product scratched from the TiO_2 film were analyzed by TEM, as shown in Fig. S3. The TEM images revealed that several nanoneedles were stacked together to form a flower-like structure. The TiO_2 film was also analyzed by atomic force microscopy (AFM) to provide further insights and obtain quantitative information about the film roughness (Fig. 2b). The average root-mean-square roughness for an area of $5 \times 5 \mu\text{m}^2$ was 14.7 nm, which was propitious for the deposition of perovskite [28]. The morphology of the perovskite films based on the SAH- TiO_2 film is presented in Fig. S4. The surface exhibited a uniform morphology with dense grains. The entire film was composed of a homogeneous well-crystallized perovskite layer, with crystalline grain lengths on the order of hundreds of nanometers. This may have been induced by the smooth morphology of the SAH- TiO_2 film, which was beneficial for the growth of perovskite layers. More details about the crystal structure of the product are shown in Fig. 2c. The main diffraction peaks were observed at 27.45° , 36.08° , 41.33° , 43.82° , 54.35° , 62.74° , and 69.01° , corresponding to the (110), (101), (111), (210), (211), (002), and (301) planes, respectively, agreeing well with the rutile phase (JCPDS card No. 21-1276) [29]. X-ray photoelectron spectroscopy (XPS) was used to investigate the chemical composition of the TiO_2 film. The $\text{Ti } 2p_{3/2}$, $\text{Ti } 2p_{1/2}$, and $\text{O } 1s$ characteristic peaks of the TiO_2 film are shown in Fig. 2d. The $\text{Ti } 2p$ spectra were identical to the $\text{Ti } 2p_{3/2}$ and $2p_{1/2}$ spectra, with peaks centered at binding energies of 458.9 and 464.7 eV, respectively, typical for Ti^{4+} states. The corresponding $\text{O } 1s$ spectra showed two major peaks at 529.9 and 532.6 eV, assigned to the lattice oxygen and surface bridging oxygen, respectively [30].

In general, the thicknesses of the resulting films are affected by the concentration of the precursor solution [31]. Figure 3 shows the cross-sectional SEM images of the TiO_2 layers formed by SAH using different concentrations of a TiCl_4 aqueous solution (0.2–0.6 M). The TiO_2 nanoneedles were well developed on the FTO substrate, forming thin films with thicknesses of 20, 45, and 80 nm for TiCl_4 aqueous solution concentrations of 0.2, 0.4, and 0.6 M, respectively. The changes in the corresponding surface morphology are shown in Fig. S5. It is well known that the TiO_2 layer plays an important role in the charge collection within PSCs, where a pinhole-free layer of appropriate thickness is desirable for an effective charge extraction. A simple method to evaluate the density of pinholes within the SAH- TiO_2 layers is shown in Fig. S6 [32]. The resistance value gradually increased with the TiCl_4 precursor solution concentration owing to the increased thickness of the TiO_2 layer. Moreover, the difference between the resistance values for the Ag paste and Ag vapor treatments of the TiO_2 layers were significantly larger when the TiCl_4

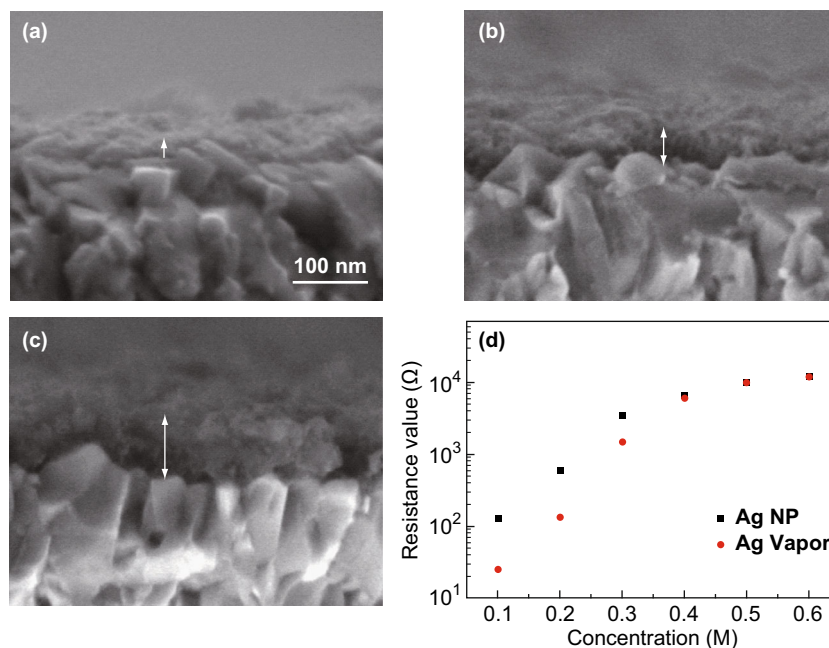


Fig. 3 Cross-sectional SEM images of the TiO₂ films prepared at different concentrations of TiCl₄ **a** 0.2 M, **b** 0.4 M, **c** 0.6 M. Panels **a–c** have the same scale-bar of 100 nm. **d** Average resistance between Ag spots on TiO₂ layers prepared using different concentrations of TiCl₄

precursor solution concentration was lower than 0.4 M. This indicated the existence of numerous pinholes. However, when the concentration of the TiCl₄ precursor solution was 0.4 M or larger, the difference between the resistance values became smaller, implying that an extremely dense TiO₂ layer was formed.

The current–voltage (*J–V*) characteristics of the perovskite cells with different SAH–TiO₂ film thicknesses obtained by varying the TiCl₄ precursor solution concentration were obtained to demonstrate the effect of the SAH–TiO₂ electron transport layers on the efficiency of the perovskite cells; the results are shown in Fig. 4. The detailed parameters are summarized in Table 1. The PCE

initially increased and then decreased with the increase of the SAH–TiO₂ layer thickness. With the 0.1-M TiCl₄ precursor solution, the coverage of TiO₂ on the FTO substrate was unsatisfactory (Fig. S5a), which increased the risk of contact between the FTO substrate and perovskite, leading to a low photovoltaic performance. With the increase of the concentration of the TiCl₄ precursor solution to 0.4 M, the coverage on the FTO substrate improved and pinholes gradually disappeared (Figs. S5b–d and 3d). Therefore, all three photovoltaic device parameters, short-circuit current density (*J_{sc}*), open-circuit potential (*V_{oc}*), and fill factor (FF), increased during this evolution process, suggesting an efficient suppression of the charge recombination on the FTO surface. The SAH–TiO₂ films (~ 45 nm) prepared by treating the FTO substrate with 0.4 M TiCl₄ exhibited the highest PCE of 17.09% with a *J_{sc}* of 21.96 mA cm⁻², *V_{oc}* of 1.069 V, and FF of 0.728. Furthermore, the integrated photocurrent from the incident photon-to-current conversion efficiency was 21.91 mA cm⁻², which is close to that from the *J–V* measurement (Fig. S8). However, a further increase in the concentration of TiCl₄ led to a deterioration of the device performance owing to the lower electron transport in the thicker TiO₂ layers and prolonged transport path, increasing the series resistance [33]. This could be confirmed by the apparent decrease in the *J_{sc}* and FF values.

It is well known that SC is only suitable for a small-area deposition simply, as the spinning rates at the core and edges significantly differ, leading to a poor uniformity of the layers in a large-area deposition. To verify this, we

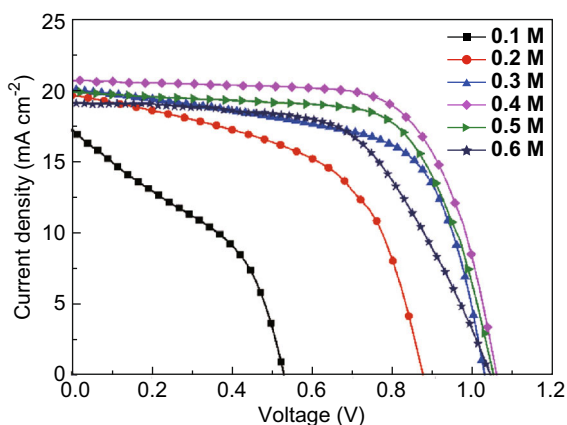


Fig. 4 *J–V* characteristics of PSCs using different concentrations of TiCl₄ to prepare the electron transport layer

Table 1 Photovoltaic parameters of SAH–TiO₂-based PSCs fabricated using the SAH method with different concentrations of TiCl₄

TiCl ₄ concentration (M)	<i>J</i> _{sc} (mA cm ⁻²)	<i>V</i> _{oc} (V)	FF	PCE (%)
0.1	18.37	0.686	0.435	5.48
0.2	20.61	0.985	0.614	12.46
0.3	21.13	1.032	0.678	14.78
0.4	21.96	1.069	0.728	17.09
0.5	20.84	1.057	0.703	15.48
0.6	19.91	1.043	0.667	13.87

attempted to deposit a TiO₂ layer on a large-area substrate (approximately 6 × 6 cm²) by SC; a reference sample prepared by SAH was used for comparison. The large coated substrates were divided into 9 small pieces (2 × 2 cm²) along the white dashed lines shown in the inset of Fig. 5a. The UV–Vis light absorption spectra of these TiO₂ films deposited by SC and SAH are shown in Fig. 5a, b, respectively. The light absorption at 320 nm was chosen as the index to determine the film uniformity as the absorption was proportional to the TiO₂ film thickness. The variation in the absorption of the SAH–TiO₂ film at 320 nm was only 6%, whereas that of the SC–TiO₂ film was 17%, which suggested that SAH was a more efficient deposition system than SC to fabricate uniform TiO₂ films. Undoubtedly, the uniformity of the TiO₂ layer influences the device performance. To illustrate this point, perovskite

devices were fabricated with small TiO₂ pieces obtained, as mentioned above. The statistical PCE distributions of 45 samples in 5 batches of PSCs based on SC–TiO₂ and SAH–TiO₂ films are shown in Fig. 5c, d, respectively. The PCE distribution of the SC–TiO₂ PSCs was broader, varying from 13.56 to 16.63%, with an average of 15.27%. In contrast, the PCE distribution of the SAH–TiO₂ PSCs was narrower (15.31–17.12%), with an average efficiency of 16.34%. Detailed information is shown in Fig. S9 and Table S1. The fluctuations in PCE for the SAH–TiO₂-based PSCs in different sub-areas were very small, indicating a higher reproducibility.

The proposed SAH method for TiO₂ film growth exhibited a remarkable uniformity over large surface areas. A 4 × 4 cm² sub-module comprising 6 cells connected in series was considered to demonstrate the consistency of the

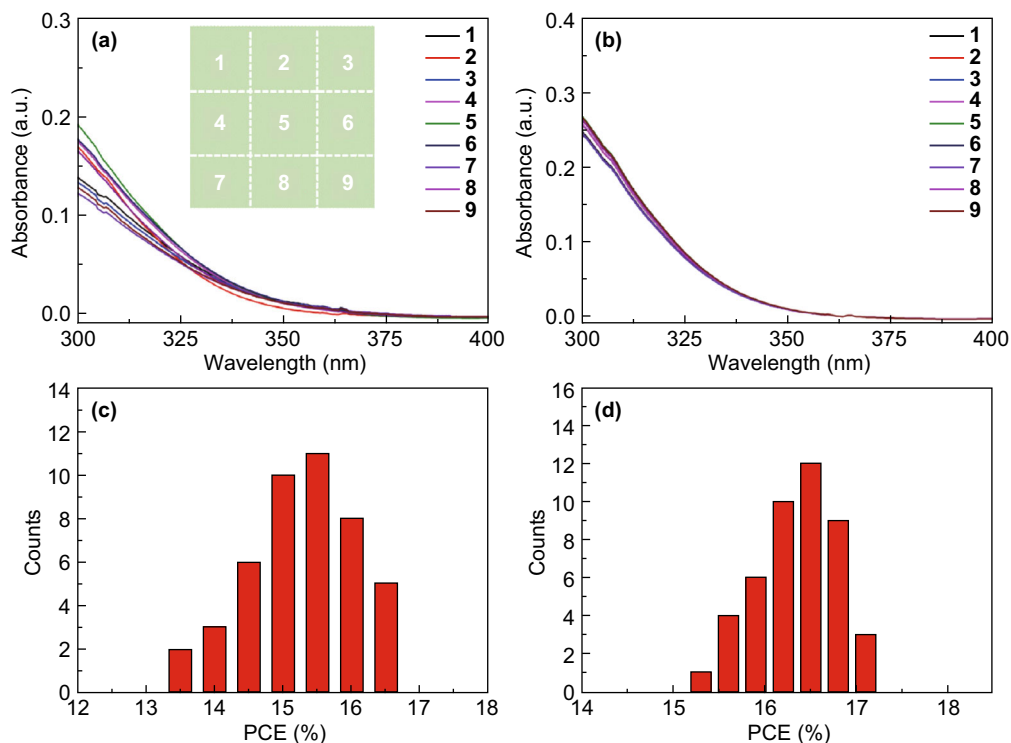


Fig. 5 UV–Vis light absorption spectra of 9 pieces of 2 × 2 cm² TiO₂ films obtained by **a** SC, **b** SAH. PCE distribution histogram of 45 **c** SC–TiO₂-based PSCs, **d** SAH–TiO₂-based PSCs. The films and PSCs were fabricated on the 9 sub-areas divided along the white dashed lines on the SC and SAH TiO₂ films (6 × 6 cm²)

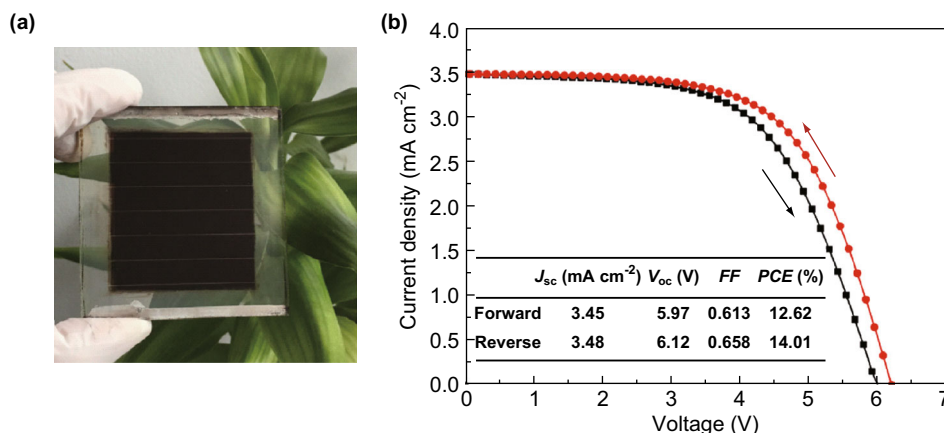


Fig. 6 **a** Photograph of the backside of the perovskite module consisting of 6 sub-cells with a total aperture area of 16 cm². **b** J - V curves of the solar module measured in forward and reverse modes under a simulated solar light of AM 1.5 G and 100 mW cm⁻²

SAH method. A photograph of the module and its J - V characteristics are shown in Fig. 6. The module exhibited V_{oc} of 6.12 V, J_{sc} of 3.48 mA cm⁻², remarkably high FF of 0.658, and overall conversion efficiency of 14.01% with hysteresis. The obtained results of the module using SAH-TiO₂ as the electron transport layer are encouraging for the development of perovskite photovoltaic technologies at low temperatures.

4 Conclusion

A simple SAH method was introduced for large-scale deposition of TiO₂ films at low temperatures. Using this method, we achieved compact homogeneous TiO₂ films with a needle-like morphology. A solar module fabricated using SAH-TiO₂ films exhibited a PCE of 14.01% with hysteresis. The results indicated that SAH is a convenient and versatile novel approach for the deposition of large-area TiO₂ films, demonstrating a large potential for practical applications in the future.

Acknowledgements This work was supported financially by the National Natural Science Foundation of China (Grants Nos. 11574199, 11674219), the Program for Professor of Special Appointment (Eastern Scholar) at Shanghai Institutions of Higher Learning, the Natural Science Foundation of Shanghai (17ZR1414800), and the Baotou-SJTU innovation guidance fund Project (17H100000514).

Open Access This article is distributed under the terms of the Creative Commons Attribution 4.0 International License (<http://creativecommons.org/licenses/by/4.0/>), which permits unrestricted use, distribution, and reproduction in any medium, provided you give appropriate credit to the original author(s) and the source, provide a link to the Creative Commons license, and indicate if changes were made.

References

- H. Zhou, Q. Chen, G. Li, S. Luo, T. Song et al., Interface engineering of highly efficient perovskite solar cells. *Science* **25**(6196), 542–546 (2014). <https://doi.org/10.1126/science.1254050>
- D. Bi, C. Yi, J. Luo, J.D. Décoppet, F. Zhang, S.M. Zakeeruddin, X. Li, A. Hagfeldt, M. Grätzel, Polymer-templated nucleation and crystal growth of perovskite films for solar cells with efficiency greater than 21%. *Nat. Energy* **1**(10), 16142–16147 (2016). <https://doi.org/10.1038/nenergy.2016.142>
- D. Liu, Y. Li, J. Yuan, Q. Hong, G. Shi et al., Improved performance of inverted planar perovskite solar cells with F4-TCNQ doped PEDOT:PSS hole transport layers. *J. Mater. Chem. A* **5**(12), 5701–5708 (2017). <https://doi.org/10.1039/C6TA10212C>
- A. Kojima, K. Teshima, Y. Shirai, T. Miyasaka, Organometal halide perovskites as visible-light sensitizers for photovoltaic cells. *J. Am. Chem. Soc.* **131**(17), 6050–6051 (2009). <https://doi.org/10.1021/ja809598r>
- F. Li, J. Yuan, X. Ling, Y. Zhang, Y. Yang, S. Cheung, C. Ho, X. Gao, W. Ma, A universal strategy to utilize polymeric semiconductors for perovskite solar cells with enhanced efficiency and longevity. *Adv. Funct. Mater.* (2018). <https://doi.org/10.1002/adfm.201706377>
- C. Zhang, Y. Luo, X. Chen, Y. Chen, Z. Sun, S. Huang, Effective improvement of the photovoltaic performance of carbon-based perovskite solar cells by additional solvents. *Nano-Micro Lett.* **8**(4), 347–357 (2016). <https://doi.org/10.1007/s40820-016-0094-4>
- Y. Li, J.K. Cooper, W. Liu, C.M. Sutter-Fella, M. Amani et al., Defective TiO₂ with high photoconductive gain for efficient and stable planar heterojunction perovskite solar cells. *Nat. Commun.* **7**, 12446 (2016). <https://doi.org/10.1038/ncomms12446>
- T. Ye, S. Ma, X. Jiang, M. Petrovic, C. Vijila, S. Ramakrishna, L. Wei, Electrospayed TiO₂ nanoporous hemispheres for enhanced electron transport and device performance of formamidinium based perovskite solar cells. *Nanoscale* **9**(1), 412–420 (2017). <https://doi.org/10.1039/c6nr07369g>
- J.-Y. Seo, R. Uchida, H.-S. Kim, Y. Saygili, J. Luo et al., Boosting the efficiency of perovskite solar cells with csbr-modified mesoporous TiO₂ beads as electron-selective contact. *Adv. Funct. Mater.* (2017). <https://doi.org/10.1002/adfm.201705763>
- NREL. *Best research-cell efficiencies*. NREL 1 (2016). http://www.nrel.gov/ncpv/images/efficiency_chart.jpg

11. C. Yang, M. Yu, D. Chen, Y. Zhou, W. Wang, Y. Li, T.C. Lee, D. Yun, An annealing-free aqueous-processed anatase TiO₂ compact layer for efficient planar heterojunction perovskite solar cells. *Chem. Commun.* **53**(79), 10882–10885 (2017). <https://doi.org/10.1039/c7cc01104k>
12. K. Wojciechowski, M. Saliba, T. Leijtens, A. Abate, H.J. Snaith, Sub-150 °C processed meso-superstructured perovskite solar cells with enhanced efficiency. *Energy Environ. Sci.* **7**(3), 1142–1147 (2014). <https://doi.org/10.1039/c3ee43707h>
13. F. Cai, L. Yang, Y. Yan, J. Zhang, F. Qin, D. Liu, Y. Cheng, Y. Zhou, T. Wang, Eliminated hysteresis and stabilized power output over 20% in planar heterojunction perovskite solar cells by compositional and surface modifications to the low-temperature-processed TiO₂ layer. *J. Mater. Chem. A* **5**(19), 9402–9411 (2017). <https://doi.org/10.1039/c7ta02317k>
14. H. Hu, B. Dong, H. Hu, F. Chen, M. Kong et al., Atomic layer deposition of TiO₂ for a high-efficiency hole-blocking layer in hole-conductor-free perovskite solar cells processed in ambient air. *ACS Appl. Mater. Interfaces* **8**(28), 17999–18007 (2016). <https://doi.org/10.1021/acsami.6b02701>
15. I.S. Kim, R.T. Haasch, D.H. Cao, O.K. Farha, J.T. Hupp, M.G. Kanatzidis, A.B. Martinson, Amorphous TiO₂ compact layers via ALD for planar halide perovskite photovoltaics. *ACS Appl. Mater. Interfaces* **8**(37), 24310–24314 (2016). <https://doi.org/10.1021/acsami.6b07658>
16. D. Yang, R. Yang, J. Zhang, Z. Yang, S. Liu, C. Li, High efficiency flexible perovskite solar cells using superior low temperature TiO₂. *Energy Environ. Sci.* **8**(11), 3208–3214 (2015). <https://doi.org/10.1039/c5ee02155c>
17. S.S. Mali, C. Hong, A.I. Inamdar, H. Im, S.E. Shim, Efficient planar n-i-p type heterojunction flexible perovskite solar cells with sputtered TiO₂ electron transporting layers. *Nanoscale* **9**(9), 3095–3104 (2017). <https://doi.org/10.1039/c6nr09032j>
18. X. Yao, J. Liang, Y. Li, J. Luo, B. Shi et al., Hydrogenated TiO₂ thin film for accelerating electron transport in highly efficient planar perovskite solar cells. *Adv. Sci.* **4**(10), 1700008 (2017). <https://doi.org/10.1002/advs.201700008>
19. X. Chen, L. Tang, S. Yang, Y. Hou, H. Yang, A low-temperature processed flower-like TiO₂ array as an electron transport layer for high-performance perovskite solar cells. *J. Mater. Chem. A* **4**(17), 6521–6526 (2016). <https://doi.org/10.1039/c6ta00893c>
20. C. Liang, Z. Wu, P. Li, J. Fan, Y. Zhang, G. Shao, Chemical bath deposited rutile TiO₂ compact layer toward efficient planar heterojunction perovskite solar cells. *Appl. Surf. Sci.* **391**, 337–344 (2017). <https://doi.org/10.1016/j.apsusc.2016.06.171>
21. P.S. Schulze, A.J. Bett, K. Winkler, A. Hinsch, S. Lee et al., Novel low-temperature process for perovskite solar cells with a mesoporous TiO₂ scaffold. *ACS Appl. Mater. Interfaces* **9**(36), 30567–30574 (2017). <https://doi.org/10.1021/acsami.7b05718>
22. A.J. Hairen Tan, O. Voznyy, X. Lan, F. Arquer, J.Z. Fan, R. Quinter, Efficient and stable solution-processed planar perovskite solar cells via contact passivation. *Science* **355**(6326), 722–726 (2017). <https://doi.org/10.1126/science.aai9081>
23. J.E. Bishop, D.K. Mohamad, M. Wong-Stringer, A. Smith, D.G. Lidzey, Spray-cast multilayer perovskite solar cells with an active-area of 1.5 cm². *Sci. Rep.* **7**(1), 7962–7973 (2017). <https://doi.org/10.1038/s41598-017-08642-2>
24. F. Ye, W. Tang, F. Xie, M. Yin, J. He et al., Low-temperature soft-cover deposition of uniform large-scale perovskite films for high-performance solar cells. *Adv. Mater.* **29**(35), 1701440 (2017). <https://doi.org/10.1002/adma.201701440>
25. H. Chen, F. Ye, W. Tang, J. He, M. Yin et al., A solvent- and vacuum-free route to large-area perovskite films for efficient solar modules. *Nature* **550**, 92–95 (2017). <https://doi.org/10.1038/nature23877>
26. M. Yin, F. Xie, X. Li, Y. Wu, X. Yang et al., Accurate and fast evaluation of perovskite solar cells with least hysteresis. *Appl. Phys. Express* **10**(7), 076601 (2017). <https://doi.org/10.7567/apex.10.076601>
27. F. Ye, H. Chen, F. Xie, W. Tang, M. Yin et al., Soft-cover deposition of scaling-up uniform perovskite thin films for high cost-performance solar cells. *Energy Environ. Sci.* **9**, 2295–2301 (2016). <https://doi.org/10.1039/c6ee01411a>
28. X. Zhang, J. Ye, L. Zhu, H. Zheng, X. Liu, X. Pan, S. Dai, High consistency perovskite solar cell with a consecutive compact and mesoporous TiO₂ film by one-step spin-coating. *ACS Appl. Mater. Interfaces* **8**(51), 35440–35446 (2016). <https://doi.org/10.1021/acsami.6b11860>
29. J. Lim, J. Pyo, D. Jung, H.-S. Jung, J.-K. Lee, Preparation of mono-dispersed spherical titania nanoparticles with precise size control using ethylene glycol. *J. Sol-Gel. Sci. Technol.* **79**(1), 89–97 (2016). <https://doi.org/10.1007/s10971-016-4005-4>
30. J. Su, L. Guo, High aspect ratio TiO₂ nanowires tailored in concentrated hcl hydrothermal condition for photoelectrochemical water splitting. *RSC Adv.* **5**, 53012–53018 (2015). <https://doi.org/10.1039/c5ra06149k>
31. A. Yella, L.P. Heiniger, P. Gao, M.K. Nazeeruddin, M. Gratzel, Nanocrystalline rutile electron extraction layer enables low-temperature solution processed perovskite photovoltaics with 13.7% efficiency. *Nano Lett.* **14**(5), 2591–2596 (2014). <https://doi.org/10.1021/nl500399m>
32. Y. Wu, X. Yang, H. Chen, K. Zhang, C. Qin et al., Highly compact TiO₂ layer for efficient hole-blocking in perovskite solar cells. *Appl. Phys. Express* **7**(5), 052301 (2014). <https://doi.org/10.7567/apex.7.052301>
33. J. Choi, S. Song, M.T. Horantner, H.J. Snaith, T. Park, Well-defined nanostructured, single-crystalline tio electron transport layer for efficient planar perovskite solar cells. *ACS Nano* **10**(6), 6029–6036 (2016). <https://doi.org/10.1021/acs.nano.6b01575>